Appl. Phys. A 63, 117–121 (1996)

Applied Physics A Materials Science & Processing

Picosecond laser ablation of thin copper films

J. Jandeleit[1], G. Urbasch[1], H.D. Hoffmann[1], H.-G. Treusch[2], E.W. Kreutz[1]

[1]Lehrstuhl für Lasertechnik, RWTH Aachen, Steinbachstrasse 15, D-52074 Aachen, Germany
(Fax: + 49-241/8906-121)
[2]Fraunhofer-Institut für Lasertechnik, Steinbachstrasse 15, D-52074 Aachen, Germany
(Fax: + 49-241/8906-121)

Received: 23 February 1996/Accepted: 11 March 1996

Abstract. The ablation process of thin copper films on fused silica by picosecond laser pulses is investigated. The ablation area is characterized using optical and scanning electron microscopy. The single-shot ablation threshold fluence for 40 ps laser pulses at 1053 nm has been determinated to $F_{thres} = 172\ mJ/cm^2$. The ablation rate per pulse is measured as a function of intensity in the range of 5×10^9 to $2 \times 10^{11}\ W/cm^2$ and changes from 80 to 250 nm with increasing intensity. The experimental ablation rate per pulse is compared to heat-flow calculations based on the two-temperature model for ultrafast laser heating. Possible applications of picosecond laser radiation for microstructuring of different materials are discussed.

PACS: 81.60.B; 79.20.D

Processing with laser radiation is influenced by a variety of parameters originating from the parameters of laser radiation, properties of material, processing conditions and environment. For thermal processing with laser radiation the interaction of laser radiation with material involves absorption of radiation with subsequent rapid thermalisation of the absorbed optical energy resulting possibly in heating, melting, vaporization or removal of material from the interaction zone as melt, vapor or plasma. The parameters of the laser radiation and the properties of the material govern the possible physical processes such as optical absorption, heat conduction, phase transitions, fluid-mechanics, evaporation kinetics and plasma dynamics, which altogether result in the output properties of the processed material.

The ablation dynamics of electrons, ions and melt particles have been investigated for picosecond pulses by several groups [1–3]. Electron and ion emission from an aluminium surface irradiated by picosecond laser pulses have been measured using time-of-flight spectroscopy [1]. Electron emission is found to dominate and only singly charged ions are detected if no plasma is created in front of the surface. Plasma expansion induced by picosecond laser radiation is also investigated by time-of-flight spectroscopy [2]. These time and angle resolved measurements show two distinct ion and electron populations. Faster species show a broad angular distribution, while slow species show a forward peaked distribution in space. The ablation of free-standing metal films was visualized by electron microscopy [3]. Hole opening was observed within 5–30 ns, speeding up with increasing laser fluence. At large fluences the evaporation was collimated along the film axis. Melt expulsion was detected.

Compared to nano- and microsecond laser pulses picosecond laser pulses change the physical conditions during material processing in different ways. Picosecond laser pulses cause a much lower heat load and reduced heat affected zone. Because of the short pulse length higher intensities can be reached and rapid heating can possibly lead to an earlier evaporation of the material and to a reduction of the molten zone which resolidifies after the end of the laser pulse at the edges of the ablated area. Therefore, picosecond laser pulses seem to offer new opportunities as a tool microstructing of different materials [4]. Holes and groves with dimensions of a few microns can be produced and thin layers can be removed ultraprecisely. These applications require an exact knowledge of the ablation behaviour as a function of laser parameters.

In the present work the ablation behaviour of thin copper films on fused silica induced by picosecond laser pulses is presented. The ablation rate per pulse is measured as a function of laser intensity and compared with heat flow calculations basing on the two-temperature model for ultrafast laser heating.

1 Fundamentals

Material processing with nanosecond and longer laser pulses is governed by a relatively slow heating process where the deposition of optical energy can be assumed to be instantaneous. For material heating by picosecond and femtosecond laser pulses this assumption is no longer valid. The finite time needed to convert optical energy absorbed by the electrons of the material to internal

energy of the lattice must be considered. Therefore, ultrafast laser heating of metals must be described by three processes: the deposition of optical energy in the electron-gas, the transport of energy by electrons and the heating of the lattice through electron-phonon interactions [5, 6].

In the IR wavelength regime the absorption of laser radiation in metals occurs by exitation of free electrons. These excited electrons occupying high energy levels thermalize rapidly by electron-electron collisions and form a hot free electron gas. The time constant describing the energy transfer the electron gas to the lattice is longer than the electron-electron scattering time. Depending on the physical properties of the material, heating rates, e.g., pulse lengths exist where a thermal equilibrium between the electron gas and the lattice cannot be assumed any longer. Based on the theory of energy transfer from electron gas to the lattice [7] Anisimov et al. [8] suggested a generalisation of the heat flow equation which can be written in the one dimensional case

$$c_E \frac{\partial T_E}{\partial t} = \nabla \cdot (K \nabla T_E) - G(T_E - T_L) + S, \tag{1a}$$

$$c_L \frac{\partial T_L}{\partial t} = G(T_E - T_L). \tag{1b}$$

The absorbed laser energy acts as a source S for the heating of the electron gas. It is assumed that the thermalisation of the electrons appears on such a short time scale, that the electron gas can be described by the temperature T_E. The heat flow is governed by the temperature gradient of the electron gas. The thermal conductivity K is determinated by the electrons. The thermal current resulting from phonons is neglected. Via electron–phonon interaction which is described by a coupling constant G, the energy is given to the lattice which is characterized by the temperature T_L c_L and c_E are the heat capacities of the electron gas and the lattice, respectively.

In the case of thermal equilibrium between electron gas and lattice (1a) and (1b) are equivalent to the standard heat flow equation [9]. Due to the short pulse length according to Bechtel [10] the source term is given as a volume source.

Equations (1a) and (1b) have been used to calculate the temperature of samples in femtosecond heating experiments of metals [11, 12]. Satisfactory agreement theory and experiment in low exitation experiments ($T_E < 1000$ K) is found. The characterisation of the hot electron gas by a temperature T_E is valid except for early times after the pulse, where in femtosecond experiments the electron gas is not yet thermalized [13]. Wang et al. have given some corrections to describe experiments with higher excitation levels [14] but the knowledge about the heating mechanisms is not sufficient to describe the ablation experiments, especially because phase transitions and evaporation are not taken into account.

In addition, the knowledge of physical properties in this high temperature regime is very poor. Furthermore, thin metal films are characterised by physical properties that differ from those of the bulk material. As an example Qiu and Tien [15] describe the influence of film thickness and grain size on the thermal conductivity of metal films. Experimentally, the thermal conductivity can be determined via the measurement of the electric conductivity by using the Wiedemann-Franz law.

Material parameters play an important role for the description of the ablation process. Ablation by laser radiation is associated with a threshold fluence depending on laser material parameters. Ablation only takes place, if the applied fluence is above the threshold fluence. For the determination of the threshold fluence holes are drilled into the material. The intensity distribution of the laser radiation in connection with the applied determinates the diameter of these laser drilled holes. For a Gaussian beam profile the measured hole diameters, $2r_d$, are related to the threshold fluence F_{thres} [16] via

$$F_{thres} = F \exp(-r_d^2/2r_f^2) \tag{2a}$$

or

$$r_d^2 = 2\, r_f^2\, [\ln(F) - \ln(F_{thres})], \tag{2b}$$

where F is the applied fluence and r_f the focus radius. If r_d^2 is plotted vs $\ln(F)$ an extrapolation to $r_d^2 = 0$ yields the threshold fluence.

2 Experimental setup

Picosecond laser pulses were generated by a diode-pumped modelocked Nd:YAG laser producing pulses with a length of 40 ps, a single pulse energy of 8 nJ and a repetition rate of 120 MHz. These low energy pulses were amplified by a diode-pumped regenerative amplifier leading to a maximum pulse energy of 200 µJ at the sample surface [17]. The repetition rate of the amplified pulses was 750 Hz. The pulse length was measured with an autocorrelator. A single 40 ps pulse was separated from the pulse train by a Pockels cell, expanded and finally focused onto the thin copper films by an ULWD (Ultra Large Working Distance) microscope objective. The working distance was 8 mm. The Pockels cell also suppressed pre- and post-pulses. The intensity distribution of the laser radiation was monitored by a CCD camera. A Gaussian intensity distribution was detected. The diameter of the focused spot was determined by the wedge method. Using this method a $1/e^2$ focus radius of 3.1 µm was measured. The samples were mounted on an XYZ-stage allowing to expose each pulse to a virgin surface. The integration of the focussing optics into an optical microscope permits the direct observation of the processed area. The experimental setup including the laser beam path is shown in Fig. 1. Copper films of 1 µm thickness, which are deposited on fused silica by thermal vaporization, were used for the investigations. The ablated areas were characterized by Scanning Electron Microscopy (SEM).

3 Experimental results

In the investigated intensity regime of 5×10^9–2×10^{11} W/cm^2, the films were not completely removed from the

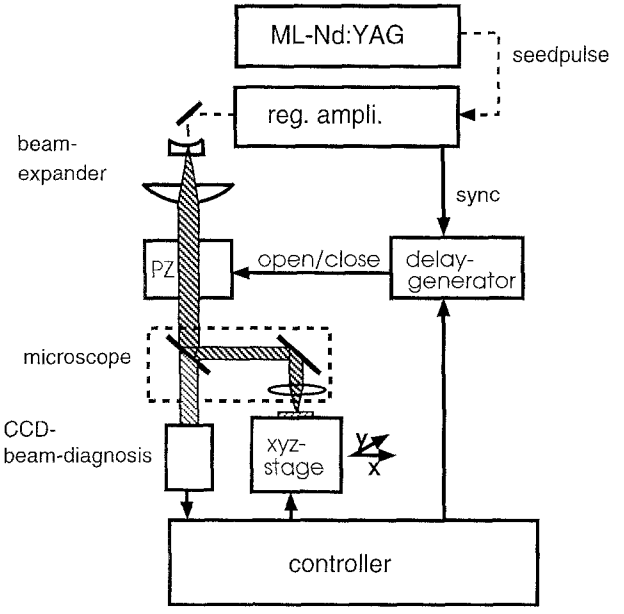

Fig. 1. Experimental setup

substrate by one laser pulse and the holes show a circular geometry in accordance to the spatial Gaussian intensity distribution. At low laser intensities no redeposition of ablated material in the surrounding area of the laser drilled holes can be detected (Fig. 2). The walls of the holes are covered with a thin molten film. The thickness of this film is 75–100 nm for a laser intensity of 1.1×10^{10} W/cm^2 and 200 nm for a laser intensity of 1.7×10^{10} W/cm^2, respectively. These resolidified films indicate the existence of a sharp boundary between molten and non-molten material by picosecond laser processing of metals.

The single-shot ablation threshold fluence for 40 ps laser pulses at a wavelength of 1053 nm was determined for thin copper films to $F_{\text{thres}} = 172$ mJ/cm^2 (Fig. 3).

The ablation rate per pulse as a function of intensity was determined for copper films on fused silica by measuring the number of laser pulses needed to remove the complete film from the substate. In the investigated intensity regime of 5×10^9–2×10^{11} W/cm^2, the ablation rate per pulse differs from 80 to 250 nm (Fig. 4). The experimental errors result from the used method for the determination of the ablation rate, because it is not known at which time during the last laser pulse the film is completely removed from the substrate.

4 Discussion

For 40 ps laser pulses the ablation of metals is still a thermal process. Optical energy is absorbed by the free electrons and transfered to the lattice by electron-phonon coupling. The electron–phonon relaxation time τ of metals is of the order of a few picoseconds [18]. After this relaxation time electrons are in thermal equilibrium with the lattice. If the applied fluence is above a certain threshold fluence the material will be removed by evaporation and melt expulsion.

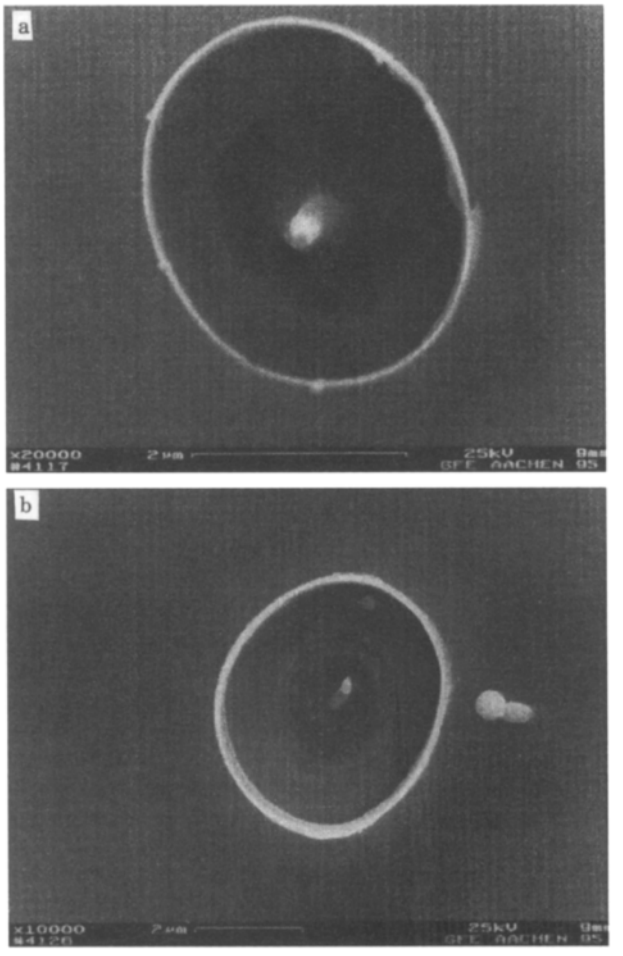

Fig. 2a,b. SEM images of laser-drilled holes, 1 pulse, $t_p = 40$ ps, $\lambda = 1053$ nm; **(a)** $I = 1.1 \times 10^{10}$ W/cm^2, $F = 0.4$ J/cm^2, $d_m = 3$ µm; **(b)** $I = 1.7 \times 10^{10}$ W/cm^2, $F = 0.7$ J/cm^2, $d_m = 4$ µm

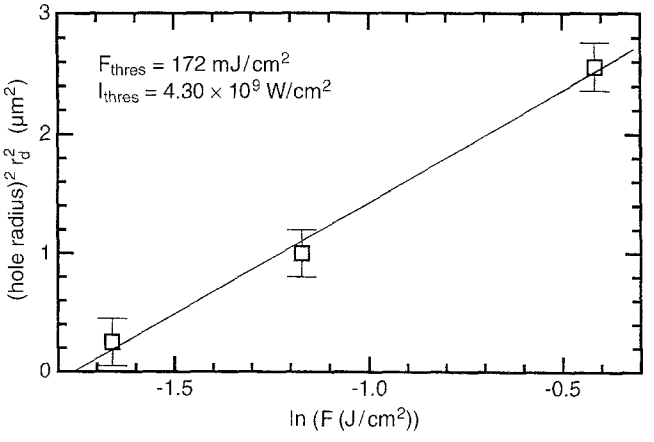

Fig. 3. Square of hole radius as a function of the logarithm of fluence, $t_p = 40$ ps, $\lambda = 1053$ nm, $r_f = 3.1$ µm

From the morphology of the ablated area (Fig. 2) conclusions can be drawn on the ablation mechanisms. The features in the middle of the holes indicate resolidified material. These features result from the strong material removal from the middle of the hole and indicate the

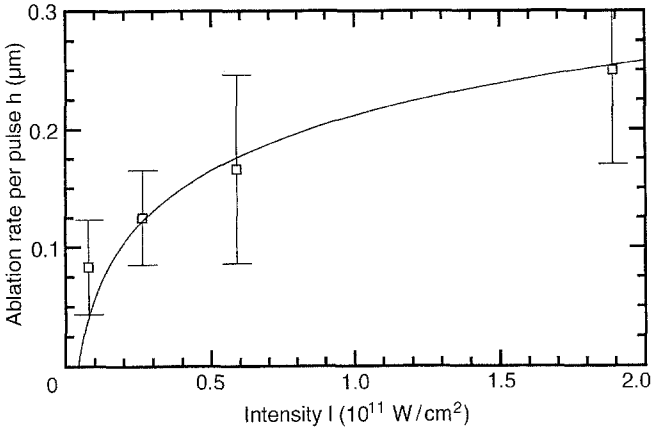

Fig. 4. Ablation rate per pulse as function of intensity for copper; $t_p = 40$ ps, $\lambda = 1053$ nm, $r_f = 3.1$ μm

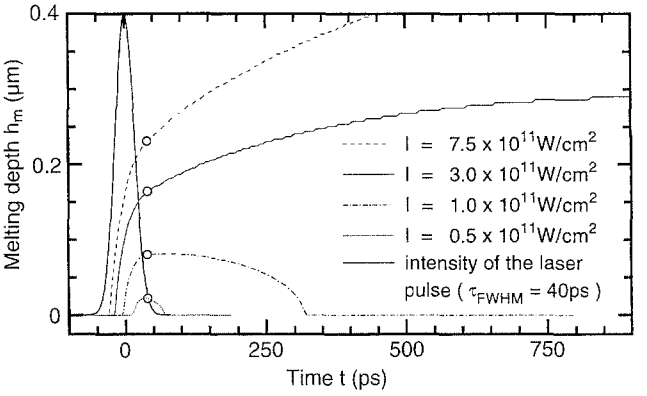

Fig. 5. Calculated depth where the sample is at melting temperature as function of time. The temporal intesity profile of the laser is shown. The circles mark the melting depths at $t_0 = 40$ ps

collimation of the ablated particles along the axis of the incoming laser beam. The ring-shaped films at the walls of the holes are formed through melt expulsion by the vapor pressure. Outside the holes this melt expulsion results in ultrathin free-standing films. Radial melt splashes or debris are not found in the surrounding area.

Compared to ablation thresholds of metal films for nanosecond laser pulses [19] the measured ablation threshold for picosecond laser pulses is decreased by one order of magnitude. The experimentally observed low threshold fluence of 172 mJ/cm^2 for ablation is due to the reduced heat losses into the surrounding material governed by the short pulse length. This value is comparable to the numerical value of the sub-picosecond threshold for copper found by Preuss et al. [20]. But this sub-picosecond threshold is related to the evaporation, while the picosecond ablation threshold presented in this paper is related to the melting of the material. The picosecond ablation threshold for evaporation would be higher due to the thermal heat of evaporation. Following these considerations, the ablation threshold for evaporation would be higher for picosecond laser pulses than for femtosecond laser pulses.

Nevertheless for picosecond ablation processes heat conduction into the sample plays an important role. The thermal conductivity K of thin metal films can differ from the bulk thermal conductivity and must be considered. Therefore, the thermal conductivity of the thin copper films used in the investigations was determined by measuring the electrical conductivity and using Wiedemann-Franz law. A value of $K_{film} = 1.70$ W/cm K was found for the thermal conductivity which is approximately half the bulk value of $K_{bulk} = 3.85$ W/cm K.

In the regime of picosecond material ablation the rate of ablated material is small compared to ns-ablation and high compared to femtosecond experiments [20]. While with nanosecond laser pulses the material is continuously ablated during the pulse, femtosecond experiments show that the ablation rate is determined by the optical penetration depth of the laser radiation in the material. Because of the exponential decay according to Beer's law the ablation rate per pulse h [20] is given by

$$h = (1/\alpha)\ln(F/F_{thres,fs}), \tag{3}$$

where $1/\alpha$ is the optical absorption length and $F_{thres,fs}$ the threshold fluence for femtosecond ablation.

In Fig. 4, the solid line is a fit according to (3), where the experimentally determinated threshold value for the 40 ps pulses is used and $1/\alpha$ is the only adjustable parameter. The optical absorption length of copper at 1053 nm is 14 nm. Using a value of $1/\alpha = 67$ nm leads to an excellent agreement between the experimental result and the fitting curve. The value of 67 nm is approximately the heat penetration depth for 40 ps pulses according to the definition $\sqrt{\kappa t_p}$, where κ is the thermal conductivity and t_p is the pulse length, respectively. This indicates that for picosecond material ablation heat conduction determinates the ablation depth.

The measured ablation rates are compared with calculated melt depths because, due to the complete expulsion of the melt by the evaporation pressure, the ablation rate should be determinated by the melt depth. Therefore, (1a) and (1b) are solved in one dimension with the method of finite differences on a nonuniform grid of 300 points. The grid is finest at the surface side because of the steep gradients imployed by the small optical absorption depth of metals. Except for the measured thermal conductivity and a reflectivity $R = 0.97$ measured by optical spectroscopy, constant bulk physical properties and a laser pulse of Gaussian shape in time with a Full Width at Half Maximum (FWHM) of $t_p = 40$ ps are used in the calculation. The intensity maximum is reached at $t = 0$ ps. The starting time of the calculation is assumed to be at negative times at three times the FWHM of the pulse so that the heating by the leading edge of the pulse is taken into account. The melting enthalpy of the sample is neglected. The calculations provide the temperature of the electron gas and the lattice depending on space and time.

In Fig. 5, the depth is shown where the sample is at melting temperature as a function of time for five intensities. Similar curves result for the evaporation temperature. The depth in which the melting temperature is reached grows while the laser pulse hits the sample. For intensities smaller than 5.3×10^{11} W/cm^2 the depth reduces after an intensity dependent maximum has been reached. This is due to the heat flow away from the surface of the sample. The heat is conducted into the depth of the sample

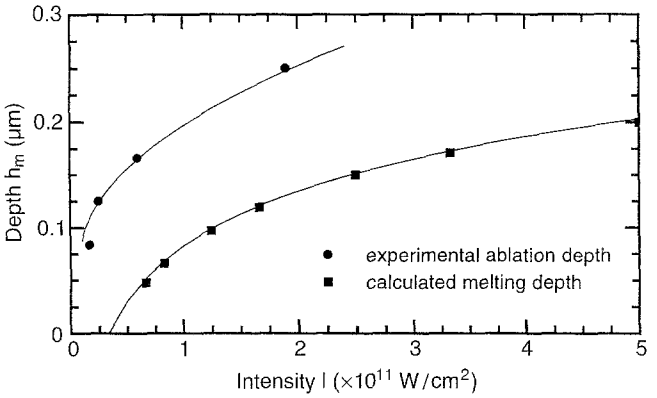

Fig. 6. Calculated melting depth as function of intensity according to Fig. 5. The calculated depths were fitted using (3). The experimentally determined ablation depths are given for comparison. The *line* through the experimental points is to guide the eye

and the region near the surface is getting cooler. For higher intensities, the depth in which the melting temperature is reached grows continuously until the backside of the film is reached. In this case, the energy deposited in the film with a finite thickness of 1 μm is sufficient to melt the whole film.

In the calculation dissipative processes are not incorporated. For example the vaporisation at the front of the sample would reduce the heat flow into the sample. For picosecond laser pulses evaporation starts already during the laser pulse [21]. Therefore, the melting depth at $t_0 = 40$ ps is taken as an estimate for the ablation depth because significant vaporisation should occur at this time. In Fig. 5, the melt depths at this time are marked by circles. This means, the vaporisation pressure is responsible for the expulsion of the melt in agreement with the SEM characterisation of the laser-drilled holes. Furthermore, at that time the melting depth should not grow any longer because of the energy loss due to vaporisation.

The choice of $t_0 = 40$ ps is somewhat arbitrary but the evaluation leads to principally the same result if the time t_0 is varied in the range from 40 to 120 ps.

Figure 6 depicts the melting depths found by the upper method. The fits according to (3) are done by adjusting both free parameters, F_{thres} and $1/\alpha$. The dependence on the intensity is very similar to the experimental result and the ablation depth is of the same order of magnitude.

With regard to the poor knowledge about physical properties and the simple assumption for the interpretation of the ablation process, which is the base for the calculation, there is a reasonable agreement with the experimental result.

The presented results show the possibilities of picosecond laser pulses as a tool for microstructuring of metals. Ultraprecise removal of thin layers with sub-micron resolution can be achieved, in agreement with heat flow calculations. The lateral precision of the ablated area is determined by thin molten films of 75–200 nm thickness, which separate the ablated areas from the remaining material.

5 Conclusion

The ablation process of thin copper films on fused silica by picosecond laser pulses was studied. SEM characterisation of laser-drilled holes show thin molten films of 75–200 nm thickness at the walls of the holes and no redeposition of ablated material in the surrounding area. The ablation threshold fluence for the copper films was measured to $F_{\text{thres}} = 172$ mJ/cm^2, which is one order of magnitude below the threshold fluence for nanosecond laser pulses. The ablation rate per pulse is in the range of 80–250 nm in the investigated intensity regime of 5×10^9 to 2×10^{11} W/cm^2. The experimental ablation rate was compared to heat flow calculations based on the two-temperature model for ultrafast laser heating. The calculated melt depths show a reasonable agreement with the experimental ablation rate and support the mechanism of strong melt expulsion by picosecond laser ablation, as seen by SEM.

Acknowledgement. We acknowledge financial support by the BMBF-Verbund Projekt "PROBE", 13N6157.

References

1. P. Martin, R. Trainham, P. Agostini, G. Petite: Phys. Rev. B **45**, 69 (1992)
2. W. Marine, M. Gerri, P. Thomsen-Schmidt, J.M. Scotto d' Aniello: Appl. Surf. Sci. **69**, 290 (1993)
3. O. Bostanjoglo, R. Niedrig, B. Wedel: J. Appl. Phys. **76**, 3045 (1994)
4. J. Jandeleit, G. Urbasch, D. Hoffmann, H.-G. Treusch, E.W. Kreutz: Proc. Laser 95 (Springer Berlin, Heidelberg) (in press)
5. H. Kurz, L.A. Lompré, J.M. Liu: J. Phys. (Paris) C **5**, 23 (1983)
6. H. Kurz: Mater. Res. Soc. Symp. Proc. **74**, 3 (1987)
7. M.I. Kaganov, I.M. Lifshitz, L.V. Tanatarov: Sov. Phys. -JETP **4**, 173 (1957)
8. S.I. Anisimov, B.L. Kapeliovich, T.L. Perel'man: Sov. Phys. -JETP **39**, 375 (1974)
9. H.S. Carslaw, J.C. Jaeger: *Conduction of Heat in Solids* (Oxford Univ. Press London 1959)
10. J.H. Bechtel: J. Appl. Phys. **46**, 1585 (1975)
11. J.G. Fujimoto, J.M. Liu, E.P. Ippen, N. Bloembergen: Phys. Rev. Lett. **53**, 1873 (1984)
12. R.W. Schoenlein, W.Z. Lin, J.G. Fujimoto, G.L. Eesley: Phys. Rev. Lett. **58**, 1680 (1987)
13. W.S. Fann, R. Storz, H.W.K. Tom, J. Broker: Phys. Rev. Lett. **68**, 2834 (1992)
14. X.Y. Wang, D.M. Riffe, Z.-S. Lee, M.C. Downer: Phys. Rev. B **50**, 8016 (1994)
15. T.Q. Qiu, C.L. Tien: J. Heat Transfer **115**, 842 (1993)
16. C.A. MacDonald, A.M. Malvezzi, F. Spaepen: *Beam-Solid interactions and Phase Transformations*, ed. by H. Kurz, G.L. Olsen, J.M. Poate Mater. Res. Soc. Symp. Proc., Vol. 51, (1986) pp. 277–282
17. H.D. Hoffman, H.-G. Treusch, E.W. Kreutz: Proc. Laser 95 (Springer Berlin, Heidelberg) (in press)
18. B. Hüttner, G. Rohr. Appl. Surf. Sci. (in press)
19. E. Matthias, M. Reichling, J. Siegel, O.W. Käding, S. Petzoldt, H. Skurk, P. Bizenberger, E. Neske: Appl. Phys. A **58**, 129 (1994)
20. S. Preuss, A. Demchuk, M. Stuke: Appl. Phys. A **61**, 33 (1995)
21. G. Urbasch, J. Jandeleit, H.-G. Treusch, E.W. Kreutz: Pro. ECLAT 96, ed. by H.W. Bergmann, F. Daasinger (RWT Wiesbaden) (in press)